Braiding of Majorana zero modes
Topological Insulators 2 (Topological superconductors)
Lecture 6, 2020/04/01

For this week, there are two pre-lecture reading assignments: to read the topocondmat chapter on braiding (*Why Majoranas are cool: braiding and quantum computation*), and to read the first 3 pages of these notes. Please read the topocondmat chapter first, and these notes second.

I. AN IMPORTANT CONTROL QUESTION TO THE TOPOCONDMAT CHAPTER

Question: Consider a system with only one pair of Majorana modes, thus with two degenerate ground states, having different fermion parity. When we exchange the two Majorana modes, starting from a given fermion parity eigenstate, the wave function picks up a phase that depends on the fermion parity. What is this phase for the even state, what is it for the odd state, and what is the relative phase between the two phases?

Answer: The individual phases are not well defined, but the relative phase is $\pi/2$. This can be deduced from the 4×4 matrix U_{12} in section *Non-Abelian statistics of Majoranas*.

II. SUMMARY

On `topocondmat.org`, you have read a high-level description of the braiding of Majorana zero modes, and how that can be used to perform nontrivial quantum operations in the degenerate ground state of topological superconductor wires. You might now wonder about the following questions:

(i) I'd like to write a numerical simulation of braiding of Majorana zero modes in such a wire network. What is the simplest time-dependent Hamiltonian that can be used for this? How would I confirm in the simulation that the difference of the phases picked up by the even and odd ground states is $\pi/2$?

(ii) What is the minimal model of an actual experimental setup and experimental protocol which could be used to prove that braiding indeed provides a $\pi/2$ gate?

In these notes, we will focus on these types of questions, and in particular, try to outline an answer to (ii), along with a numerical demonstration of the experimental setup and protocol we propose.

III. BALL-AND-STICK MODEL OF A TOPOLOGICAL QUANTUM BIT

Here we introduce a ball-and-stick model of a topological quantum bit that is based on Majorana zero modes. This takes simple quantum information protocols we've learned in Lecture 3, such as non-protected Rabi oscillations and readout via parity-to-charge conversion, and combines it with braiding, which you've just read about on `topocondmat.org`.

The setup is sketched in Fig. 1. It consists of 3 units: a *readout dot* (black), a *Y junction* built from Kitaev chains (sites (1,1), (0,0), (3,1),(2,1)), and a further *straight Kitaev chain* (sites (-1,1), (-1,2), (-1,3)). Dashed lines denote connections via electron tunneling and Cooper-pair creation and annihilation. Solid lines denote connections via tunneling only.

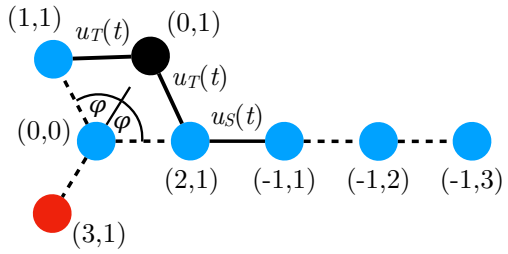

FIG. 1: Ball-and-stick model of a topological quantum bit, 'designed' for an experimental demonstration of the braiding-based quantum gate. In the simulations, we will set $\varphi = \pi/2$ for concreteness.

Before proposing and specifying the experimental protocol that could be used to demonstrate a braiding-based quantum gate, let's discuss the role of each unit of our lattice model.

The Y junction and the straight Kitaev chain can both be regarded as fermion-parity pseudoqubits, and their composite system creates a Majorana qubit. By default, both the Y junction and the straight Kitaev chain are tuned to their topological fully dimerized limit, and hence the ground state of their composite system is fourfold degenerate. The four ground states will be denoted as $|ee\rangle$, $|eo\rangle$, $|oe\rangle$, $|oo\rangle$, with e (o) being a reference to the even (odd) fermion-number parity of each unit.

The experimental protocol to demonstrate braiding consists of two subprotocols A and B, A is where no braiding is applied, and B is where braiding is applied. The steps of subprotocol B are similar to those of a so-called Ramsey experiment:

1. **Initialization.** To, say, $|ee\rangle$. This limits the physically available ground state to the globally even two-dimensional subspace of $|ee\rangle$ and $|oo\rangle$.
2. **First qubit rotation.** A non-protected $\pi/2$ gate is performed around the 'y axis', by switching on the tunnel coupling u_S between the sites (2,1) and (-1,1) for an appropriate duration, see Lecture 3. This step will prepare a balanced superposition $(|ee\rangle + |oo\rangle)/\sqrt{2}$.
3. **Braiding.** Braiding of the Majorana zero modes localized on sites (1,1) and (2,1), making use of the red site (3,1) of the Y junction. This will create a phase difference in the superposition, $(|ee\rangle + e^{i\pi/2}|oo\rangle)/\sqrt{2}$.
4. **Second qubit rotation.** A second non-protected $\pi/2$ gate around the y axis. This will leave the state as it is.
5. **Readout.** It is performed using the black readout dot (0,1), in the way explained in Lecture 3 - by switching on the two tunnel couplings u_T for an appropriate duration, and reading out the charge of the readout dot afterwards. This will read out the parity of the Y junction, and hence will find $|e\rangle$ and $|o\rangle$ with 50%-50% probability.

This 50%-50% outcome of subprotocol B should be contrasted to the outcome of subprotocol A. In the latter, the only difference is that in step (3) we don't do a braiding, but just do nothing instead. Then, the final state will be $|oo\rangle$ and the readout outcome will be 100% for $|o\rangle$ and 0% for $|e\rangle$. So, we conclude that doing protocols A and B should indeed confirm that braiding produces a $\pi/2$ gate on the Majorana qubit.

IV. NUMERICAL DEMONSTRATION OF THE BRAIDING-BASED QUANTUM GATE

The results of our numerical simulation of the above protocol are shown in Fig. 2. Focus on Fig. 2a for concreteness. Here, we plot the average occupation of the readout dot at the end of subprotocol B, as a function of the duration of the braiding (step (3)). We use unites defined by $\hbar = 1$ and $v = \Delta = 1$, where $v = \Delta$ is the single energy scale characterizing the topological fully dimerized Kitaev chains. As noted above, the readout dot occupation carries the parity information of the Y junction: if it's zero, that signals that the Y junction was in the even state before starting the parity-to-charge conversion, if it's one, that signals the odd parity. Our expectation described above, that a very slow (adiabatic) braiding does a $\pi/2$ gate and hence makes the average readout dot occupation $1/2$ is indeed confirmed by the result in Fig. 2a.

You might wonder: is an average dot occupation of $1/2$ a satisfying signature of a precisely functioning quantum gate? Isn't it possible that we get $1/2$ as a result of some wild decoherence mechanism which randomizes the Majorana qubit during the braiding, step (3)?

To check that scenario, we also do the simulation for a third subprotocol, call it C, where we do two subsequent braidings in step (3). The result of this is shown in Fig. 2d. As you see, the result of the two braidings is that the final dot occupation is zero, that is, the final state of the Majorana qubit is $|ee\rangle$. This is indeed what we expect from two subsequent braidings: we initialize in $|ee\rangle$, do a $\pi/2$ rotation around y, then two braidings providing a π rotation around z, and another $\pi/2$ rotation around y, so we end up in $|ee\rangle$ where we started. Hence, the simulation of subprotocol C in Fig. 2d does confirm that braiding behaves as expected.

Note that in these two plots Fig. 2a,d also illustrate that braiding works only for long-enough braiding times, here for $T \gtrsim 100$, as there's a significant deviation from the expected outcome for shorter braiding times.

V. DISORDER-INDUCED ERRORS IN THE BRAIDING PROTOCOL.

At the end of the topocondmat chapter, it is argued that the motivation to study these complicated quantum systems is that the Majorana qubit is more robust against uncontrolled imperfections than standard qubits. Furthermore, the

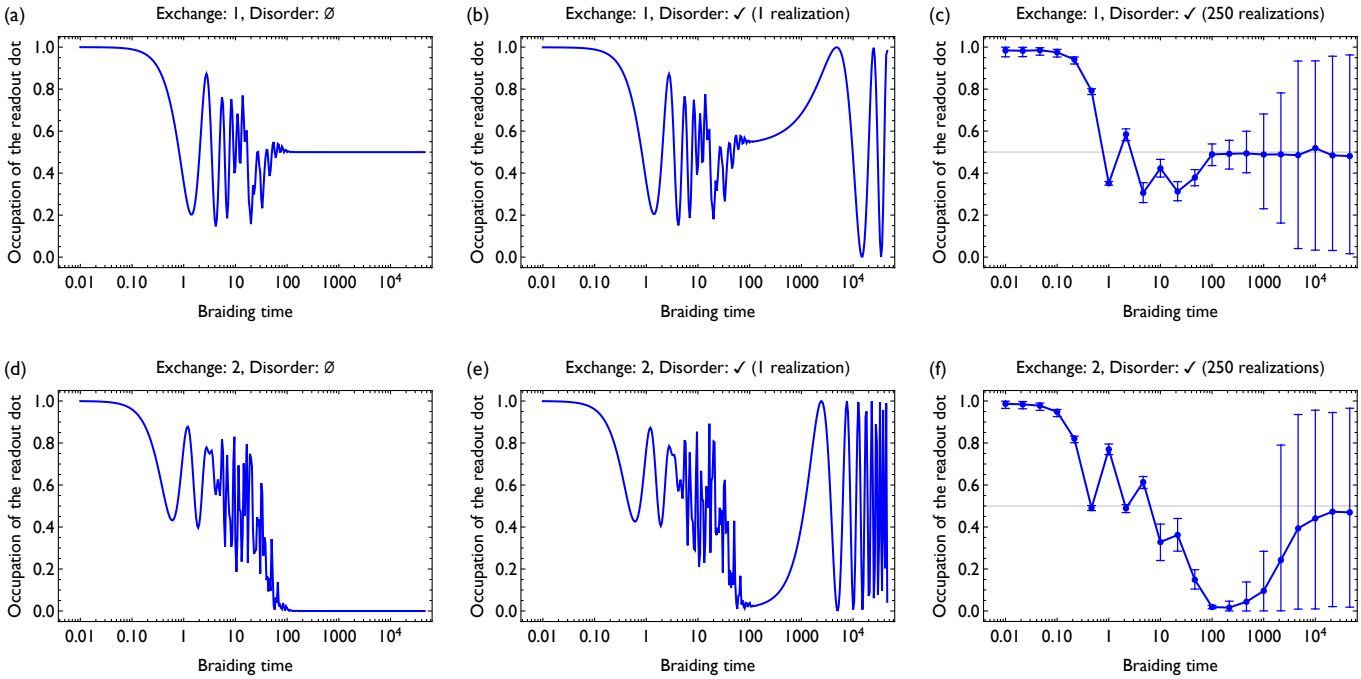

FIG. 2: Numerical simulation of an experimental protocol demonstrating a braiding-based quantum gate.

braiding-based $\pi/2$ gate is also more robust than a standard quantum gate. It is interesting to use our numerical simulations to investigate that claim.

What we do in our numerics will not be sufficient for a demonstration of 'topological protection' of the braiding-based quantum gate. For that, we'd need to show that the gate errors get exponentially suppressed as the length of the Kitaev chains is increased, which we do not do here. Nevertheless, let's see what we get in our case of a fixed-sized, rather small, model.

The 'imperfection' we study here is disorder: We assume that we set our system in the topological fully dimerized limit, but there is also an unwanted and uncontrolled static contribution to each parameter of the Hamiltonian (hopping, pair potential, chemical potential/on-site energy) which are represented as independent Gaussian random variables with standard deviation of 0.05 (in units of $v = \Delta$).

In Fig. 2b, we show the occupation of the readout dot at the end of the single-braiding subprotocol B, as the function of the braiding time. One feature we observe is that the short-braiding-time segment $T \lesssim 100$, the data looks very similar to the clean case of Fig. 2a. For longer braiding times, we first see the ideal occupation value $1/2$ appearing around braiding time ≈ 100, but we also see the occupation strongly deviating from that ideal value for longer braiding times.

Why do we see these drastic error levels for long braiding times, where we expected to see the ideal, adiabatic behavior? This is because disorder detunes the Kitaev chains from the fully dimerized limit, causing Majorana hybridization and minigaps both in the Y junction and in the straight Kitaev chain. As a consequence of the minigaps, the dynamical phases picked up by the even and odd ground states become nonzero, and cause significant deviations from the ideal adiabatic scenario, which is relying only on the geometric phase difference $\pi/2$ between the even and odd ground states. The role of the dynamical phase is further illustrated by the fact that the occupation shows oscillations for long braiding times $T \gtrsim 10^4$.

The remaining three plots further explore the role of disorder. Fig. 2e: shows the result of subprotocol C (two braidings). Fig. 2c shows the disorder-averaged result of subprotocol B, averaging 250 different disorder realizations. Fig. 2f shows the disorder-averaged result of subprotocol C.

What is your expectation? What would change in these figures, if we'd change the length of the Kitaev chains from 3 to, say, 10?

How would you generalize this protocol to make use of the continuum of qubit rotation angles in steps 2 and 4?

Appendix A: Contributors

Writeup: Péter Boross, András Pályi. Simulations: Péter Boross. Discussions, ideas: János Asbóth, László Oroszlány, Gábor Széchenyi.

Appendix B: Literature

The key paper introducing the braiding-based quantum gate in topological superconducting wire networks is J. Alicea et al., Nature Physics 2011. Another very relevant paper, showing numerical simulations of braiding, albeit without disorder and without explicitly describing a measurement protocol, is Sekania et al., arXiv:1703.03360. Further nice reviews: Leijnse & Flensberg arXiv:1206.1736, Hassler arXiv:1404.0897, Beenakker arXiv:1907.06497.

Appendix C: Details of the model and the simulation

In these appendices, we provide details of the model and simulations discussed above in the main text.

The setup is shown in Fig. 1. The Y junction consists of three regular Kitaev chains and a central site. Each Kitaev chain can be described by the following Hamiltonian:

$$H_c^{(n,N_c)} = \sum_{i=1}^{N_c-1} \left(v c_{n,i}^\dagger c_{n,i+1} + \Delta_n c_{n,i}^\dagger c_{n,i+1}^\dagger + \text{h.c.} \right) + \sum_{i=1}^{N_c} \mu_{n,i}(t) c_{n,i}^\dagger c_{n,i}, \tag{C1}$$

where N_c is the length of the chain, $c_{n,i}^\dagger$ and $c_{n,i}$ are the creation and annihilation operators on the ith site of the nth chain, v denotes the nearest-neighbor hopping amplitude, Δ_n is the p-wave superconducting pairing amplitude in the nth chain, and $\mu_{n,i}(t)$ is the site-dependent potential. In the main text, we consider only $N_c = 1$, when the first term of Eq. (C1) is zero, and only the second term exists.

The Hamiltonian of the complete Y junction reads

$$H_Y = \sum_{n=1}^{3} H_c^{(n,N)} + \mu_{0,0} c_{0,0}^\dagger c_{0,0} + \sum_{n=1}^{3} \left(v c_{0,0}^\dagger c_{n,1} + \Delta_n c_{0,0}^\dagger c_{n,1}^\dagger + \text{h.c.} \right), \tag{C2}$$

where index $(0,0)$ denotes the central site, and the superconducting pair potential is $\Delta_1 = \Delta e^{i\varphi}$, $\Delta_2 = \Delta e^{-i\varphi}$ and $\Delta_3 = -\Delta$. The parameter φ plays a nontrivial role - but for simplicity, we disregard the dependence on φ and set it to $\pi/2$ in our simulations, which is a 'safe choice'.

The length of the straight Kitaev chain is chosen to have the same length as the topological region of the Y-junction, which is 3 in our case $N_c = 1$. Thus the corresponding Hamiltonian is

$$H_W = H_c^{(-1,2N_c+1)} = H_c^{(-1,3)}, \tag{C3}$$

where $\Delta_{-1} = \Delta e^{-i\varphi}$.

For readout, an additional site, the readout dot denoted by $(0,1)$, is coupled to the system. The Hamiltonian of the full system, consisting of 8 sites and hence 8 fermionic modes, reads:

$$H = H_Y + H_W + \mu_{0,1} c_{0,1}^\dagger c_{0,1} + \underbrace{\left(u_S(t) c_{0,1}^\dagger c_{0,2} + \text{h.c.} \right)}_{H_S} + \underbrace{\sum_{n=1}^{2} \left(u_T(t) c_{0,1}^\dagger c_{n,N} + \text{h.c.} \right)}_{H_T}. \tag{C4}$$

Here, $u_S(t)$ is the hopping amplitude between the rightmost site of the Y junction and the leftmost site of the straight Kitaev chain, which is required in steps 2 and 4 of the experimental protocol outlined in the main text. Furthermore, $u_T(t)$ is the tunneling amplitude between the readout dot and the two ends of the Y-junction, which is utilized for parity-to-charge conversion in step 5 of the experimental protocol.

Appendix D: Experimental protocol / subprotocol B

Here we provide more details on the numerical simulation of the experimental protocol outlined in the main text. We focus on subprotocol B, and subprotocol C is done analogously.

1. **Initialization.** Th readout dot is empty, and uncoupled from the Y junction. The Y junction and the straight Kitaev chain are uncoupled. The topological region of the Y-junction is defind by the sites $(1,1)$, $(0,0)$ and $(2,1)$. A substantial on-site potential is switched on on site $(3,1)$. The ground state of the system is fourfold degenerate: $|\mathrm{e},\mathrm{e},0\rangle$, $|\mathrm{o},\mathrm{o},0\rangle$, $|\mathrm{e},\mathrm{o},0\rangle$, $|\mathrm{o},\mathrm{e},0\rangle$, where the first (second) character corresponds to the fermion-number parity of the Y junction (straight Kitaev chain), and the third argument to the occupation of the readout dot. We assume we have initialized in the system in the ground state $|\mathrm{e},\mathrm{e},0\rangle$.

2. **First qubit rotation.** By turning on the tunneling $u_S(t)$ between the Y-junction and the wire for a certain time, we can implement rotation in the (Majorana qubit) subspace spanned by the states $|\mathrm{e},\mathrm{e},0\rangle$ and $|\mathrm{o},\mathrm{o},0\rangle$ in the even sector. The switching on/off can be instantaneous, or smooth:

$$u_S(t) = u_S\Theta(t)\Theta(\tau_S - t), \tag{D1a}$$
$$u_S(t) = u_S\Theta(t)\Theta(\tau_S - t)\sin^2(\pi t/\tau_S), \tag{D1b}$$

   The duration τ_S of the pulse is set to make a $\pi/2$ rotation around the qubit y axis. To achieve that, instantaneous switching requires $\tau_S = \pi/(4u_S)$, smooth switching requires $\tau_S = \pi/(2u_S)$. In the simulations shown in the main text, we use the smooth pulse.

3. **Braiding.** Spatial exchange of the Majorana zero modes can be performed in the Y-junction. These modes can be moved along the chains by changing the on-site potentials. The exchange takes τ_E time, and realizes a $\pi/2$ rotation over the Z axis. For details, see Sekania et al., arXiv:1703.03360.

4. **Second qubit rotation.** We apply a second $\pi/2$ rotation around the y axis.

5. **Reaodut.** By turning on the two hopping amplitudes u_T between the readout dot and the ends (Majorana zero modes) of the Y junction, we perform parity-to-charge conversion from the Y junction to the dot charge. The switching on/off can be instantaneous or smooth (with, e.g., sine-squared ramp):

$$u_T(t) = u_T\Theta(t - 2\tau_S - \tau_E)\Theta(2\tau_S + \tau_T + \tau_E - t), \tag{D2a}$$
$$u_T(t) = u_T\Theta(t - 2\tau_S - \tau_E)\Theta(2\tau_S + \tau_T + \tau_E - t)\cdot\sin^2\left[\pi\left(t - 2\tau_S - \tau_E\right)/\tau_T\right]. \tag{D2b}$$

   In the simulations, we use the smooth version, which is better as it stirs up significantly less quasiparticles than the square-like kick. To achieve nominally perfect parity-to-charge conversion, instantaneous switching requires $\tau_T = \pi/(4u_T)$, smooth switching requires $\tau_T = \pi/(2u_T)$. At the end of the parity-to-charge conversion, the occupation of the readout dot is measured.

The hopping and the pair potential in the Y junction and in the straight Kitaev chain are tuned as in the topological fully dimerized limit: $v = \Delta$. Only the on-site energies of the Y junction are changed during the braiding, with values varying between $\mu = 0$ and $\mu = 4\Delta$.

Appendix E: Effective Hamiltonians

The coupling between the Y-junction and the wire (H_S), and the coupling between the Y-junction and the readout dot (H_T) can be written in the even parity sector on the $\{|\mathrm{e},\mathrm{e},0\rangle, |\mathrm{o},\mathrm{o},0\rangle, |\mathrm{e},\mathrm{o},1\rangle, |\mathrm{o},\mathrm{e},1\rangle\}$ basis, and in the odd parity sector on the $\{|\mathrm{e},\mathrm{e},0\rangle, |\mathrm{o},\mathrm{o},0\rangle, |\mathrm{e},\mathrm{o},1\rangle, |\mathrm{o},\mathrm{e},1\rangle\}$ basis:

$$(H_S + H_T)|_{\mathrm{e}} = \begin{pmatrix} 0 & \frac{1}{4}i\left(u_S^* + u_S\right) & 0 & 0 \\ -\frac{1}{4}i\left(u_S^* + u_S\right) & 0 & -u_T & 0 \\ 0 & -u_T^* & 0 & -\frac{1}{4}\left(u_S^* + u_S\right) \\ 0 & 0 & -\frac{1}{4}\left(u_S^* + u_S\right) & 0 \end{pmatrix} \tag{E1}$$

$$(H_S + H_T)|_{\mathrm{o}} = \begin{pmatrix} 0 & \frac{1}{4}\left(u_S^* + u_S\right) & 0 & 0 \\ \frac{1}{4}\left(u_S^* + u_S\right) & 0 & -u_T & 0 \\ 0 & -u_T^* & 0 & -\frac{1}{4}i\left(u_S^* + u_S\right) \\ 0 & 0 & \frac{1}{4}i\left(u_S^* + u_S\right) & 0 \end{pmatrix} \tag{E2}$$

Appendix F: Wave functions in the idealized experimental protocols

In Table I, we collect the wave functions after the different operations for subprotocols A, B, C, in the ideal scenario.

	A (0× braiding)	B (1× braiding)	C (2× braiding)
Initialization	$\|\mathrm{e},\mathrm{e},0\rangle$		
First qubit rotation	$\frac{1}{\sqrt{2}}\|\mathrm{e},\mathrm{e},0\rangle + \frac{1}{\sqrt{2}}\|\mathrm{o},\mathrm{o},0\rangle$		
Braiding	$\frac{1}{\sqrt{2}}\|\mathrm{e},\mathrm{e},0\rangle + \frac{1}{\sqrt{2}}\|\mathrm{o},\mathrm{o},0\rangle$	$\frac{1}{\sqrt{2}}\|\mathrm{e},\mathrm{e},0\rangle + \frac{i}{\sqrt{2}}\|\mathrm{o},\mathrm{o},0\rangle$	$\frac{1}{\sqrt{2}}\|\mathrm{e},\mathrm{e},0\rangle - \frac{1}{\sqrt{2}}\|\mathrm{o},\mathrm{o},0\rangle$
Second qubit rotation	$\|\mathrm{o},\mathrm{o},0\rangle$	$\frac{1-i}{2}\|\mathrm{e},\mathrm{e},0\rangle + \frac{1+i}{2}\|\mathrm{o},\mathrm{o},0\rangle$	$\|\mathrm{e},\mathrm{e},0\rangle$
Readout	$i\|\mathrm{e},\mathrm{o},1\rangle$	$\frac{1-i}{2}\|\mathrm{e},\mathrm{e},0\rangle - \frac{1-i}{2}\|\mathrm{e},\mathrm{o},1\rangle$	$\|\mathrm{e},\mathrm{e},0\rangle$

TABLE I: Development of the wave function at the key points of the subprotocols A, B,C, involving 0, 1, and 2 braidings.